RESEARCH ARTICLE | MARCH 12 2025

Numerical analysis of hybrid electromagnetic coil designs for efficient gradient field generation in magnetic particle imaging

Special Collection: 16th Joint MMM-Intermag Conference

Shahriar Mostufa ; Ebrahim Azizi ; Bahareh Rezaei; Changzhi Li ; Jenifer Gómez-Pastora ; Rui He ; Kai Wu

AIP Advances 15, 035217 (2025)
https://doi.org/10.1063/9.0000854

Numerical analysis of hybrid electromagnetic coil designs for efficient gradient field generation in magnetic particle imaging

Cite as: AIP Advances 15, 035217 (2025); doi: 10.1063/9.0000854
Submitted: 1 November 2024 • Accepted: 28 January 2025 •
Published Online: 12 March 2025

Shahriar Mostufa,[1,a)] Ebrahim Azizi,[1] Bahareh Rezaei,[1] Changzhi Li,[1] Jenifer Gómez-Pastora,[2] Rui He,[1] and Kai Wu[1,a)]

AFFILIATIONS

[1] Department of Electrical and Computer Engineering, Texas Tech University, Lubbock, Texas 79409, USA
[2] Department of Chemical Engineering, Texas Tech University, Lubbock, Texas 79409, USA

Note: This paper was presented at the 16th Joint MMM-Intermag Conference.
[a)] **Authors to whom correspondence should be addressed:** smostufa@ttu.edu and kai.wu@ttu.edu

ABSTRACT

Magnetic particle imaging (MPI) is an emerging tomographic imaging modality that has shown great potential for cell tracking, tumor imaging, gut bleeding, etc. As MPI moves towards clinical applications, one challenge faced by this technology is the increasing power consumption for field generation as the bore size increases. Joining the efforts in transitioning MPI to clinical applications, especially for human-sized MPI. Herein, using COMSOL Multiphysics, we numerically studied three coil designs for generating high gradient fields with high field uniformity at lower power consumption. Specifically, the Maxwell electromagnetic (EM) coils, the hybrid EM coils with an NdFeB magnet core, and the hybrid EM coils with an NdFeB magnet core designed as a magnetic flux concentrator (MFC). We first compared the efficiency of these three coil designs in generating gradient fields by evaluating the maximum gradient field strength and field uniformity. With the same current applied to these coils, the hybrid EM coils with a NdFeB MFC core show the best gradient field profiles, achieving a maximum gradient field strength of 5 T/m. The current supplied to these EM coils and the coil winding layers are varied to study their effects on the gradient field profiles. Additionally, the geometrical parameter of the MFC structure is optimized, and we have achieved a maximum gradient field strength of 5 T/m over a 14.3 cm space, with a tolerance of 98%.

I. INTRODUCTION

Magnetic particle imaging (MPI) is a tracer-based, noninvasive, tomographic imaging modality first reported in 2005 by Gleich and Weizenecker.[1] In an MPI system, an alternating magnetic field (AMF, excitation field) periodically magnetizes the magnetic nanoparticle (MNP) tracers and causes the nonlinear magnetic responses that are recorded by a pair of receiver coils.[2–4] To realize tomographic imaging, spatial encoding is achieved by adding a gradient field that selectively "enables" the magnetic responses of tracers within a field-free region (FFR) while "disables" (or magnetically saturating) tracers outside this FFR. The field of view (FOV) is determined by the ratio of excitation field amplitude to the gradient field strength.[5] To date, the reported gradient field strength is typically in the range of 1 to 7 T/m/μ_0.[6–12] A higher gradient field strength favors a smaller FFR, thus, a higher imaging resolution can be achieved. However, in the meantime, the higher gradient field strength also reduces the range of FOV.[5,13,14] To solve this issue, focus fields are often added to increase the spatial coverage for scanning a larger object, such as a human-sized MPI scanner.[15–18]

Another challenge in transitioning MPI to clinical applications with large bore sizes is achieving lower power consumption, higher gradient field strength, and better field uniformity across the FOV.[19–21] Ensuring gradient field uniformity throughout the entire FOV is crucial, but this becomes increasingly difficult as the FOV increases.[20,22] For instance, Irfan *et al.* reported a hybrid

electromagnetic (EM) coil design using COMSOL modeling, which incorporated both a permanent magnet as a core and an EM coil to generate the gradient field.[23] However, their design only achieved a maximum gradient field strength of 4.3 T/m, with a uniformity of 4 cm (with a 96.8% homogeneity). Recently, Tian *et al.* reported that by using a superconductor, a high gradient field can also be generated with fewer coil windings.[24] However, the current required for powering the gradient field coils increases enormously, which can only be achieved with the superconductors. Making it difficult for their design to transition to clinical settings, especially in resource-limited regions.

This work aims to search for an energy-efficient way to generate sufficiently high gradient field strengths that provide the maximum field uniformity in FOV. We first designed three different hybrid EM coils and analyzed their gradient field profiles using the finite element method in COMSOL. Then, we extended our analysis to study the impact of various parameters of these EM coils, including current and number of coil windings and geometrical parameters of the MFC. Our results show that under the same conditions, the hybrid EM coils with an NdFeB core designed as a magnetic flux concentrator (MFC) provide the highest gradient field strength of 5 T/m, in comparison to 2.3 T/m and 4.4 T/m obtained from EM coils and EM coils with an NdFeB core, respectively. We further optimized the geometrical designs on the MFC by varying the top surface diameter from 0 cm (cone) to 50 cm (cylinder), with the aim of achieving the highest field uniformity across 14.3 cm FOV.

II. DESIGN METHODOLOGY

In this work, we have designed the Maxwell EM coil [Fig. 1(a)], the hybrid Maxwell EM coil with an NdFeB core [Fig. 1(b)], and the hybrid Maxwell EM coil with an NdFeB core designed as a magnetic flux concentrator [MFC, Fig. 1(c)], for gradient field generation. The parameters for the EM coil and MFC are labeled in Fig. 1(d). The COMSOL Multiphysics software was used to study the magnetic flux density profiles inside the FOV. The EM coil and MFC parameters and their values modeled in this work are shown in Table I.

TABLE I. The EM coil and MFC parameters and values used in this work.

Parameters	Values
Outer radius of EM coil (r_1)	31.8 cm
Inner radius of EM coil (r_2)	25 cm
Space between two Maxwell EM coils (d)	20 cm
Wire diameter (w_d)	1.7 mm
Number of coil windings per layer	117
Total number of coil windings (N) = windings per layer × number of layers	4680
Coil length (l) >= windings per layer × wire diameter	20 cm
Number of layers (L)	40
Top diameter of the MFC (a)	22 cm
Height of the MFC (h)	5 cm
The inner diameter of EM coil and the bottom diameter of the MFC (g)	50 cm
Coil thickness = outer radius − inner radius = wire diameter × number of layers	6.8 cm
Current supplied to EM coils	45 A

In the COMSOL, we used the AC/DC module and stationary study solver to conduct the numerical analysis of the magnetic flux produced by these three sets of coil designs. The Maxwell EM coils were supplied with DC currents in opposite directions. The magnetic field physics module was used, and the EM coils were modeled as homogenized multi-turn, circular coil types. Additionally, we used the infinite element domain surrounding the coils as a boundary condition. We have used the materials from the existing COMSOL material library - Copper, Air, and the permanent magnet NdFeB (material code: BMN-35). For the NdFeB core, the remanent flux density was used in the modeling. Finally, we used a "physics-controlled mesh" module with a finer element size for the meshing. The gradient field strength along the z-direction inside the FOV is recorded by measuring the magnetic flux density, B_z, calculated by $G_z = \frac{\partial B_z}{\partial z}$.[5]

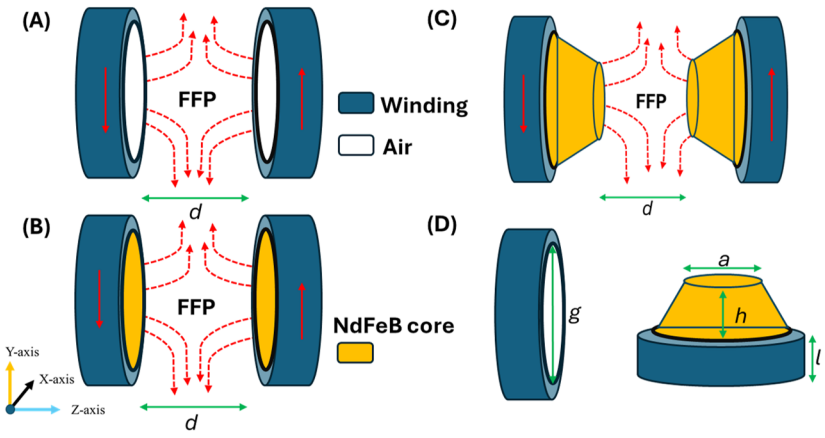

FIG. 1. Schematics of different EM coil designs modeled in this work. (a) EM coil. (b) Hybrid EM coil with an NdFeB core. (c) Hybrid EM coil with an NdFeB core designed as MFC. (d) Definitions of coil parameters.

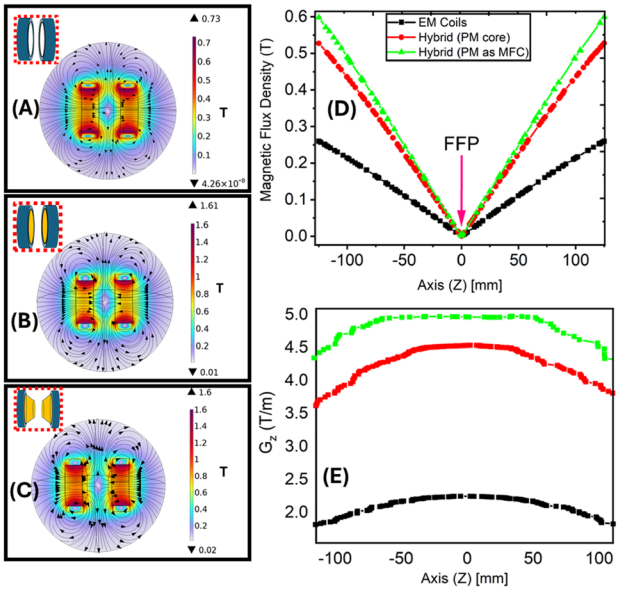

FIG. 2. The magnetic flux density in the COMSOL modeling space produced by (a) EM coils, (b) hybrid EM coils with NdFeB core, and (c) hybrid EM coils with NdFeB core designed as MFC. The magnetic flux density (d) and the gradient field strength G_z (e) are plotted along the z-axis.

III. RESULTS AND DISCUSSIONS

A. The magnetic flux density and gradient field strength profiles

Figures 2(a)–2(c) depict the generated magnetic flux density, from the EM coil, the hybrid EM coil with an NdFeB core, and the hybrid EM coil with an NdFeB core designed as MFC, respectively. The generation of the FFP is demonstrated for each of the three coil types, as seen in Figs. 2(a)–2(c).

The magnetic flux along the central z-axis line of FOV is plotted in Fig. 2(d). A stepper magnetic flux is observed from the hybrid EM coils with an NdFeB core designed as MFC, in comparison with the EM coils and the hybrid EM coils with an NdFeB core. An FFP, labeled in Fig. 2(d), located in the center of the Maxwell coils, is identified from all three sets of gradient field coils.

Finally, the gradient field profiles, calculated from the slope of magnetic flux density, are plotted in Fig. 2(e). With the same current applied, coil windings, and all other identical parameters (shown in Table I), the hybrid EM coils with an NdFeB core designed as MFC can provide a higher gradient field with better field uniformity compared to the other two configurations. From Fig. 2(e), we can see the maximum gradient field strengths generated by three coil configurations are 2.3 T/m, 4.4 T/m, and 5 T/m, respectively. The field uniformity is defined considering a tolerance of 98% of the maximum gradient field strength. From Fig. 2(e), the

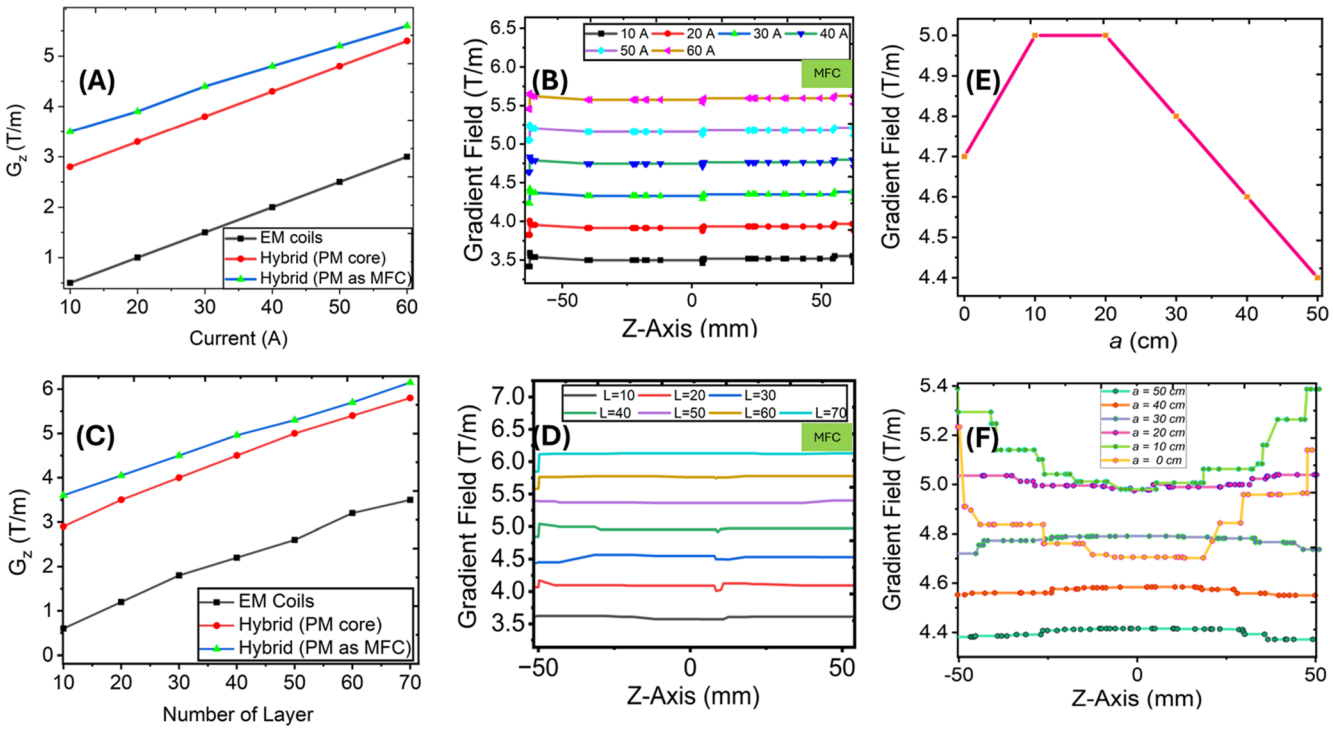

FIG. 3. The maximum gradient field strengths recorded from three different coil designs as we vary the (a) current and the (c) number of coil layers. The gradient field profiles (G_z) along the Z-axis are plotted in (b) and (d), corresponding to (a) and (c), respectively. (e) The maximum gradient field strengths are recorded as we vary the top surface diameter, a, of the MFC structure. Correspondingly, the gradient field profiles along the Z-axis in the FOV are plotted in (f).

calculated gradient field uniformity space for the EM (air core), hybrid (PM core), and hybrid (PM as MFC) are 7.8, 8.3, and 14.3 cm, respectively.

B. Effect of current and winding layers on the gradient field profiles

Furthermore, for the EM coil parameters, we have varied the current and the layer of windings to study their effects on the gradient field profiles. The variations are done by fixing the other parameters identically. Figures 3(a) and 3(c) show the maximum gradient field strengths observed in the FOV as the current and number of winding layers change, respectively. It is observed that for all three coil configurations, the gradient field strength increases with the increasing current and winding layers. However, under all the conditions modeled, the hybrid EM coils with an NdFeB core designed as MFC give the highest gradient field strengths.

In addition, the gradient field strength profiles along the central z-axis are summarized in Figs. 3(b) and 3(d), respectively, as the current and number of layers vary. The hybrid EM coils with an MFC core design have shown the highest gradient field strength as well as field uniformity. Thus, in the following of this work, we only study the design of hybrid EM coils with NdFeB core designed as MFC for achieving lower power consumption, higher gradient field strength, and better field uniformity. The goal of this work is to achieve a minimum 14.3 cm gradient field uniformity in the FOV at a tolerance of 98%.

C. Effect of the MFC structural geometry on gradient field profiles

In this section, we have varied the MFC geometrical parameters to search for a gradient field generator that is more energy-efficient, has higher gradient field strength, and has better field uniformity. Specifically, the top surface diameter, a, of cone-structured NdFeB MFC, was varied from 0 cm to 50 cm, and the maximum gradient field strength, G_z, was recorded in Fig. 3(e). Where when a = 0 cm, the MFC becomes a cone structure, and when a = 50 cm, the MFC becomes a cylinder.

As the top surface diameter of MFC increases from 0 cm to 10 cm, we observed an increase in the maximum gradient field strength from 4.7 to 5.0 T/m. This maximum gradient field strength of 5.0 T/m is also observed when a = 20 cm. As we further increase the top surface diameter beyond 20 cm, the gradient field strength drops monotonically. When a = 0 cm and 10 cm, the gradient field strength profiles along the Z-axis show non-uniformity in comparison with other scenarios (a = 20, 30, 40, and 50 cm), as shown in Fig. 3(f). Although a = 10 cm and a = 20 cm both generate the same gradient field strength of 5.0 T/m, the non-uniformity of the gradient field strength profile for a = 10 cm is unfavored. Thus, the cone-structured MFC with a top surface diameter of 20 cm and bottom surface diameter of 50 cm gives us the highest and the most uniform gradient field in the FOV.

IV. CONCLUSION

Researchers in the areas of MPI design and MPI-based medical imaging are pursuing a low-energy consumption method for large-bore size imaging. Herein, using the finite element method and COMOSL Multiphysics tool, we have designed and numerically studied three kinds of EM coils for generating the gradient fields in MPI. Namely, the traditional Maxwell EM coils, the hybrid EM coils with an NdFeB core, and the hybrid EM coils with an NdFeB core designed as MFC. By setting the coil parameters and current identical (listed in Table I), the gradient field strengths of 2.3 T/m, 4.4 T/m, and 5 T/m were achieved from these three coil configurations. From the gradient field profiles within a 14.3 cm FOV, it has been found that the hybrid EM coils with an NdFeB core designed as MFC showcase not only the highest gradient field strength but also the best field uniformity. We further studied the effect of current and number of coil winding layers on the gradient field profiles of these three coil designs. Under all the scenarios we have studied, the hybrid EM coils with this MFC core design have shown the highest gradient field strength as well as field uniformity.

Finally, we focused on optimizing the geometrical parameters of the MFC with the aim of searching for higher gradient field strength and field uniformity across the FOV. As we vary the top surface diameter of the cone MFC structure, the highest gradient field strength of 5 T/m and largest field uniformity of 10 cm was achieved when a = 20 cm. This work provides peers with a solution for applying COMOSL to numerically study and design coils for higher efficiency field generation in MPI, not only for gradient fields but also for focus fields. Although the proposed MFC design is based entirely on numerical simulations, it introduces novel insights into improving MPI systems to achieve better spatial resolution and larger scanning areas.

ACKNOWLEDGMENTS

This study was financially supported by Texas Tech University through HEF New Faculty Startup, NRUF Start Up, and Core Research Support Fund. B. R. acknowledges the Distinguished Graduate Student Assistantships (DGSA) offered by Texas Tech University.

AUTHOR DECLARATIONS

Conflict of Interest

The authors have no conflicts to disclose.

Author Contributions

C.L., J.G-P., R.H., and K.W. conceived the presented idea. S.M. carried out the COMSOL modeling and led the writing of this manuscript. E.M., B.R., and K.W. supported the writing, figure plotting, and result discussions. C.L., J.G-P., R.H., and K.W. interpreted the results and proofread the manuscript.

Shahriar Mostufa: Conceptualization (equal); Data curation (equal); Formal analysis (equal); Investigation (equal); Methodology (equal); Software (equal); Writing – original draft (equal). **Ebrahim Azizi**: Writing – review & editing (supporting). **Bahareh Rezaei**: Writing – review & editing (supporting). **Changzhi Li**: Writing –

review & editing (supporting). **Jenifer Gómez-Pastora**: Writing – review & editing (supporting). **Rui He**: Writing – review & editing (supporting). **Kai Wu**: Conceptualization (equal); Writing – original draft (equal); Writing – review & editing (equal).

DATA AVAILABILITY

The data that support the findings of this study are available from the corresponding authors upon reasonable request.

REFERENCES

[1] B. Gleich and J. Weizenecker, "Tomographic imaging using the nonlinear response of magnetic particles," Nature **435**(7046), 1214–1217 (2005).

[2] K. Wu, J.-P. Wang, N. A. Natekar, S. Ciannella, C. González-Fernández, J. Gomez-Pastora, Y. Bao, J. Liu, S. Liang, X. Wu, L. Nguyen T Tran, K. Mercedes Paz González, H. Choe, J. Strayer, P. R. Iyer, J. Chalmers, V. Chugh, B. Rezaei, S. Mostufa, Z. W. Tay, C. Saayujya, Q. Huynh, J. Bryan, R. Kuo, E. Y. Yu, P. Chandrasekharan, B. Fellows, S. M. Conolly, R. L. Hadimani, A. El-Gendy, R. Saha, T. Broomhall, A. L. Wright, M. Rotherham, A. El Haj, Z. Wang, J. Liang, A. Abad-Díaz-de-Cerio, L. Gandarias, A. G. Gubieda, A. García-Prieto, and M. L. Fdez-Gubieda, "Roadmap on magnetic nanoparticles in nanomedicine," Nanotechnology **36**, 042003 (2024).

[3] B. Rezaei, P. Yari, S. M. Sanders, H. Wang, V. K. Chugh, S. Liang, S. Mostufa, K. Xu, J.-P. Wang, J. Gómez-Pastora, and K. Wu, "Magnetic nanoparticles: A review on synthesis, characterization, functionalization, and biomedical applications," Small **20**, 2304848 (2023).

[4] B. Rezaei, Z. W. Tay, S. Mostufa, O. N. Manzari, E. Azizi, S. Ciannella, H.-E.-J. Moni, C. Li, M. Zeng, J. Gómez-Pastora, and K. Wu, "Magnetic nanoparticles for magnetic particle imaging (MPI): Design and applications," Nanoscale **16**, 11802 (2024).

[5] T. Knopp and T. M. Buzug, *Magnetic Particle Imaging: An Introduction to Imaging Principles and Scanner Instrumentation* (Springer Science & Business Media, 2012).

[6] B. Zheng, M. P. von See, E. Yu, B. Gunel, K. Lu, T. Vazin, D. V. Schaffer, P. W. Goodwill, and S. M. Conolly, "Quantitative magnetic particle imaging monitors the transplantation, biodistribution, and clearance of stem cells *in vivo*," Theranostics **6**(3), 291 (2016).

[7] X. Y. Zhou, K. E. Jeffris, Y. Y. Elaine, B. Zheng, P. W. Goodwill, P. Nahid, and S. M. Conolly, "First *in vivo* magnetic particle imaging of lung perfusion in rats," Phys. Med. Biol. **62**(9), 3510 (2017).

[8] P. Szwargulski, M. Wilmes, E. Javidi, F. Thieben, M. Graeser, M. Koch, C. Gruettner, G. Adam, C. Gerloff, T. Magnus *et al.*, "Monitoring intracranial cerebral hemorrhage using multicontrast real-time magnetic particle imaging," ACS Nano **14**(10), 13913–13923 (2020).

[9] E. E. Mason, E. Mattingly, K. Herb, M. Śliwiak, S. Franconi, C. Z. Cooley, P. J. Slanetz, and L. L. Wald, "Concept for using magnetic particle imaging for intraoperative margin analysis in breast-conserving surgery," Sci. Rep. **11**(1), 13456–13516 (2021).

[10] E. Y. Yu, P. Chandrasekharan, R. Berzon, Z. W. Tay, X. Y. Zhou, A. P. Khandhar, R. M. Ferguson, S. J. Kemp, B. Zheng, P. W. Goodwill *et al.*, "Magnetic particle imaging for highly sensitive, quantitative, and safe *in vivo* gut bleed detection in a murine model," ACS Nano **11**(12), 12067–12076 (2017).

[11] J. Franke, U. Heinen, H. Lehr, A. Weber, F. Jaspard, W. Ruhm, M. Heidenreich, and V. Schulz, "System characterization of a highly integrated preclinical hybrid MPI-MRI scanner," IEEE Trans. Med. Imaging **35**(9), 1993–2004 (2016).

[12] P. W. Goodwill, E. U. Saritas, L. R. Croft, T. N. Kim, K. M. Krishnan, D. V. Schaffer, and S. M. Conolly, "X-space MPI: Magnetic nanoparticles for safe medical imaging," Adv. Mater. **24**(28), 3870–3877 (2012).

[13] N. Panagiotopoulos, F. Vogt, J. Barkhausen, T. M. Buzug, R. L. Duschka, K. Lüdtke-Buzug, M. Ahlborg, K. Lüdtke-Buzug, C. Debbeler, M. Gräser *et al.*, "Magnetic particle imaging: Current developments and future directions," Int. J. Nanomed. **10**, 3097 (2015).

[14] M. Grüttner, T. F. Sattel, M. Graeser, H. Wojtczyk, G. Bringout, W. Tenner, and T. M. Buzug, "Enlarging the field of view in magnetic particle imaging—A comparison," in *Magnetic Particle Imaging*, edited by T. M. Buzug and J. Borgert (Springer, Berlin, Heidelberg, 2012), pp. 249–253.

[15] T. Knopp, K. Them, M. Kaul, and N. Gdaniec, "Joint reconstruction of non-overlapping magnetic particle imaging focus-field data," Phys. Med. Biol. **60**(8), L15–L21 (2015).

[16] J. Borgert, J. D. Schmidt, I. Schmale, C. Bontus, B. Gleich, B. David, J. Weizenecker, J. Jockram, C. Lauruschkat, O. Mende, M. Heinrich, A. Halkola, J. Bergmann, O. Woywode, and J. Rahmer, "Perspectives on clinical magnetic particle imaging," Biomed. Eng. **58**(6), 551 (2013).

[17] N. Nothnagel, J. Rahmer, B. Gleich, A. Halkola, T. M. Buzug, and J. Borgert, "Steering of magnetic devices with a magnetic particle imaging system," IEEE Trans. Biomed. Eng. **63**(11), 2286–2293 (2016).

[18] M. Gräser, F. Thieben, P. Szwargulski, F. Werner, N. Gdaniec, M. Boberg, F. Griese, M. Möddel, P. Ludewig, and D. van de Ven, "Human-sized magnetic particle imaging for brain applications," Nat. Commun. **10**(1), 1936 (2019).

[19] P. Chandrasekharan, Z. W. Tay, X. Y. Zhou, E. Yu, R. Orendorff, D. Hensley, Q. Huynh, K. L. B. Fung, C. C. VanHook, P. Goodwill *et al.*, "A perspective on a rapid and radiation-free tracer imaging modality, magnetic particle imaging, with promise for clinical translation," Br. J. Radiol. **91**(1091), 20180326 (2018).

[20] P. Vogel, M. A. Rückert, C. Greiner, J. Günther, T. Reichl, T. Kampf, T. A. Bley, V. C. Behr, and S. Herz, "iMPI: portable human-sized magnetic particle imaging scanner for real-time endovascular interventions," Sci. Rep. **13**(1), 10472 (2023).

[21] L. Yin, W. Li, Y. Du, K. Wang, Z. Liu, H. Hui, and J. Tian, "Recent developments of the reconstruction in magnetic particle imaging," Vis. Comput. Ind. Biomed. Art **5**(1), 24 (2022).

[22] N. He, C. Xu, Z. Zhang, J. Hu, L. Li, Q. Wang, P. Guo, Y. Gao, Y. Liao, D. Ge, C. Shi, M. Luo, and S. Zhu, "A high resolution permanent magnet MPI device," Int. J. Magn. Part. Imaging IJMPI **9**(1) (2023).

[23] M. Irfan, O. Mercan Dogan, N. Dogan, and A. Bingolbali, "Selection field generation using permanent magnets and electromagnets for a magnetic particle imaging scanner," Alexandria Eng. J. **61**(10), 7685–7696 (2022).

[24] Y. Tian, S. Ma, C. Wang, and L. Fan, "Theoretical research on constructing gradient field in magnetic particle imaging system with superconductor," IEEE Trans. Appl. Supercond. **34**(8), 4905504 (2024).